

# Learning Efficient GANs using Differentiable Masks and Co-Attention Distillation

Shaojie Li<sup>1</sup>, Mingbao Lin<sup>1</sup>, Yan Wang<sup>3</sup>, Mingliang Xu<sup>4</sup>,  
Feiyue Huang<sup>5</sup>, Yongjian Wu<sup>5</sup>, Ling Shao<sup>6</sup>, Rongrong Ji<sup>1,2\*</sup>

<sup>1</sup>Media Analysis and Computing Lab, Department of Artificial Intelligence,  
School of Informatics, Xiamen University, China

<sup>2</sup>Institute of Artificial Intelligence, Xiamen University, China

<sup>3</sup>Pinterest, USA <sup>4</sup>Zhengzhou University, China <sup>5</sup>Tencent YouTu Lab, China

<sup>6</sup>Inception Institute of Artificial Intelligence, Abu Dhabi, UAE

## Abstract

Generative Adversarial Networks (GANs) have been widely-used in image translation, but their high computational and storage costs impede the deployment on mobile devices. Prevalent methods for CNN compression cannot be directly applied to GANs due to the complicated generator architecture and the unstable adversarial training. To solve these, in this paper, we introduce a novel GAN compression method, termed DMAD, by proposing a Differentiable Mask and a co-Attention Distillation. *The former* searches for a light-weight generator architecture in a training-adaptive manner. To overcome channel inconsistency when pruning the residual connections, an adaptive cross-block group sparsity is further incorporated. *The latter* simultaneously distills informative attention maps from both the generator and discriminator of a pre-trained model to the searched generator, effectively stabilizing the adversarial training of our light-weight model. Experiments show that DMAD can reduce the Multiply Accumulate Operations (MACs) of CycleGAN by  $13\times$  and that of Pix2Pix by  $4\times$  while retaining a comparable performance against the full model. Code is available at <https://github.com/SJLeo/DMAD>.

## Introduction

Generative Adversarial Networks (GANs) (Goodfellow et al. 2014) have shown predominant performance in a wide range of visual applications, such as image synthesis (Radford, Metz, and Chintala 2015), domain translation (Isola et al. 2017), image-to-image translation (Zhu et al. 2017), etc. However, the superiorities of GANs come with great costs on computational overhead and memory requirements, some of which are even an order of magnitude higher than traditional Convolutional Neural Networks (CNNs). For example, as shown in Fig.1, the popular CycleGAN (Zhu et al. 2017) requires over 56.8G MACs (Multiply-Accumulate Operations) to process a single  $256\times 256$  pixel image, which is  $13\times$  ResNet-50 (He et al. 2016) and  $189\times$  MobileNetV2 (Sandler et al. 2018). Besides, the Pix2Pix (Isola et al. 2017) also disadvantages in its number of parameters, which is  $2\times$  ResNet-50 and  $15\times$  MobileNetV2. Such a huge resource demand makes their deployment on mobile devices impractical. Thus, learning efficient GANs has become an important task in the visual community.

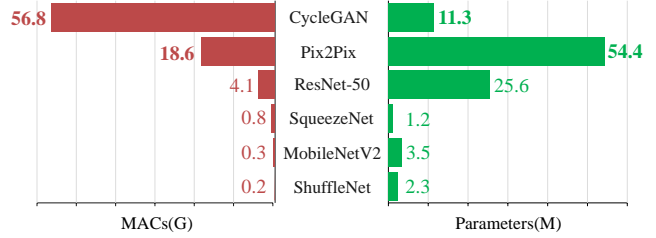


Figure 1: Comparison on MACs and parameters between GANs including CycleGAN (Zhu et al. 2017) and Pix2Pix (Isola et al. 2017), and traditional CNNs including ResNet-50 (He et al. 2016), SqueezeNet (Iandola et al. 2016), MobileNetV2 (Sandler et al. 2018) and ShuffleNet (Zhang et al. 2018). The GANs are much more complex than the traditional CNNs.

To overcome this, great effort has been made to reduce general neural network complexity, including network pruning (Ding et al. 2019; Lin et al. 2020c), weight quantization (Leng et al. 2018; Lin et al. 2020b), tensor decomposition (Denil et al. 2013; Hayashi et al. 2019), and knowledge distillation (Hinton, Vinyals, and Dean 2015; Zagoruyko and Komodakis 2017).

Among these, network pruning has attracted particular attention. Many works focus on removing individual neurons according to a given criterion, e.g., second-order Taylor expansion (LeCun, Denker, and Solla 1990),  $\ell_2$ -norm regularization (Han et al. 2015), global sparse momentum SGD (Ding et al. 2019), weight magnitude (Frankle and Carbin 2019), etc. Another group of methods remove the whole filters directly (Liu et al. 2017; Zhuang et al. 2018; Lin et al. 2020a; Wang et al. 2020). In addition to pruning, knowledge distillation (Hinton, Vinyals, and Dean 2015) has also attracted the community’s attention. By transferring knowledge from a larger teacher network, the learning ability of a smaller student network can be enhanced. To that effect, (Romero et al. 2015; Zagoruyko and Komodakis 2017; Yim et al. 2017) make full use of the intermediate representations from the teacher network to improve the performance of a student network.

While great progress has been made, the above models

\*Corresponding Author: rrji@xmu.edu.cn

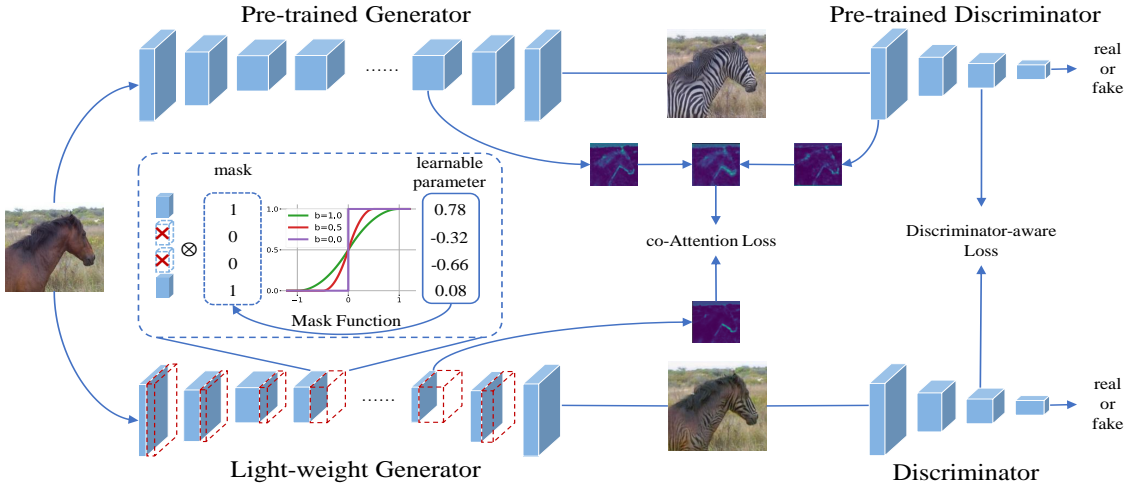


Figure 2: Framework of our DMAD. We first build a pre-trained model similar to a GAN network, upon which a differentiable mask is imposed to scale the convolutional outputs of the generator and derive a light-weight one. Then, the co-Attention of the pre-trained GAN and the outputs of the last-layer convolutions of the discriminator are distilled to stabilize the training of the light-weight model.

are specially designed for CNNs. They cannot be directly applied to GANs because of three reasons. First, different from CNNs, the generators in GANs require significantly more parameters and more complicated computation to construct high-dimensional mapping, such as image-to-image translation, style transfer, *etc.* Thus many handcrafted pruning criteria for CNNs are not compatible with GANs, and directly extending them to GANs has been demonstrated inadvisable (Shu et al. 2019; Fu et al. 2020). Second, GANs also differ from CNNs in their notorious instability of adversarial training, where the generator and discriminator are alternately updated as a two-player competition. Finally, most CNN distillation approaches only consider the final label as supervision, and thus overlook the quality and diversity of the generated images. Therefore, a GAN-specific distillation framework is necessary for effective compression.

Since recent two years, related works in this field have emerged. (Shu et al. 2019) propose to compress CycleGAN for unpaired image translation with the cycle consistency loss as the co-evolution fitness to update a sub-structure set. However, this strategy is very limited to networks with a cycle loss and cannot be straightforwardly extended to other GANs, such as Pix2Pix. (Chen et al. 2020) propose to compress GANs by distilling both the generator and discriminator information of a pre-trained model, while using a hand-crafted student generator. With the advance of network architecture search (NAS), recent works (Fu et al. 2020; Li et al. 2020) have used this to automatically derive light-weight generator models. However, this inevitably introduces high search complexity. The search space in (Fu et al. 2020) is very broad, including operations and widths that have to be pre-defined manually. Though (Li et al. 2020) incorporate once-for-all training to model a super-net and thus reduce the search complexity, the sub-net combination is still huge and results in a great burden on training. Over-

all, the above methods are either trapped in the tedious and time-consuming NAS search, or the manual design of the network which lacks flexibility. In addition, considering the diversity of the generated images, it is not wise to directly imitate the intermediate feature map or output of the pre-trained generator.

In this paper, we propose a novel GAN compression method, termed DMAD, by introducing a Differentiable Mask and co-Attention Distillation, as illustrated in Fig.2. We design a differentiable mask to carry out architecture search in a training-adaptive manner to get rid of the time-consuming NAS process and handcrafted pruning criteria. At the same time, we use the attention map of both the pre-trained generator and discriminator to stabilize the training of the light-weight generator and avoid excessive impact on the diversity of the generated results. Specifically, the convolutional outputs in the given generator network are scaled by a mask function which is differentiable in relation to its learnable input. Starting with a smooth and gentle shape, our mask can adaptively degenerate to the standard step function, in which filters with zero masks will be removed. Thus the light-weight generator can be derived automatically. However, the light-weight generator has limited performance using traditional adversarial training. Therefore we introduce a co-attention loss to provide effective supervision for a stable training process. The loss considers the attention maps of both the pre-trained generator and discriminator. Together with the feature maps from the last layer of the pre-trained discriminator, the co-attention loss guides the distillation of the light-weight generator and discriminator, which further boosts the quality of generated images.

## Methodology

GANs consist of a generator  $G$  and a discriminator  $D$ . Consider the image sets  $\mathbf{X} = \{\mathbf{x}_1, \mathbf{x}_2, \dots, \mathbf{x}_n\}$  and  $\mathbf{Y} =$

$\{\mathbf{y}_1, \mathbf{y}_2, \dots, \mathbf{y}_n\}$ , which respectively denote the source domain and target image domain. The optimization of GANs is given as:

$$\mathcal{L}_{\text{GAN}} = \mathbb{E}_{\mathbf{x}, \mathbf{y}} [\log D(\mathbf{x}, \mathbf{y})] + \mathbb{E}_{\mathbf{x}} [\log(1 - D(\mathbf{x}, G(\mathbf{x})))]. \quad (1)$$

As can be seen, the generator aims to map the source image  $\mathbf{x}$  to the target image  $\mathbf{y}$  to cheat the discriminator, while the discriminator aims to distinguish the real image  $\mathbf{y}$  from the generated image  $G(\mathbf{x})$ . Besides, for image translation, additional loss function  $\mathcal{L}_{\text{SPE}}$  is designed for the generator to complete a specific task, *e.g.*, the cycle consistency loss  $\mathcal{L}_{\text{SPE}} = \mathbb{E}_{\mathbf{x}} [\|G_2(G_1(\mathbf{x})) - \mathbf{x}\|_2]$  in CycleGAN, and the MSE loss  $\mathcal{L}_{\text{SPE}} = \mathbb{E}_{\mathbf{x}, \mathbf{y}} [\|\mathbf{y} - G(\mathbf{x})\|_1]$  in Pix2Pix. Thus, the objective of GANs for image translation is given as:

$$\mathcal{L}_{\text{cGAN}} = \mathcal{L}_{\text{GAN}} + \lambda_{\text{SPE}} \mathcal{L}_{\text{SPE}}, \quad (2)$$

where  $\lambda_{\text{SPE}}$  is a pre-given hyperparameter.

## Preliminaries

Consider a pre-trained GAN with a generator  $G_T$  and discriminator  $D_T$ . The generator  $G_T$  consists of  $L$  convolutional layers and we denote its filter weights as  $\mathbf{W}^{G_T} = \{\mathbf{W}_i^{G_T}\}_{i=1}^L$ . The  $i$ -th filter weight is given by  $\mathbf{W}_i^{G_T} \in \mathbb{R}^{n_i \times c_i \times h_i \times w_i}$ , where  $n_i, c_i, h_i$  and  $w_i$  denote the filter number, channel number, filter height and width of the  $i$ -th layer, respectively. Similarly, we have the filter weights for the discriminator  $\mathbf{W}^{D_T} = \{\mathbf{W}_i^{D_T}\}_{i=1}^L$ .

Our goal is to derive a light-weight generator  $G_S$ , filter weights of which are denoted as  $\tilde{\mathbf{W}}^{G_S} = \{\tilde{\mathbf{W}}_i^{G_S}\}_{i=1}^L$  with the  $i$ -th layer weight  $\tilde{\mathbf{W}}_i^{G_S} \in \mathbb{R}^{\tilde{n}_i \times \tilde{c}_i \times h_i \times w_i}$  under strict constraints of  $\tilde{n}_i \leq n_i$  and  $\tilde{c}_i \leq c_i$ . The set  $\{\tilde{n}_i\}_{i=1}^L$  constitutes the network architecture of the light-weight generator  $G_S$ , which should have comparable performance against the pre-trained  $G_T$  after end-to-end adversarial training.

As can be seen, deriving an outstanding light-weight  $G_S$  lies in two key points, *i.e.*, how to obtain the network architecture effectively and efficiently, and how to stabilize the adversarial training to recover the performance of the light-weight model. To this end, in what follows, we devise a differentiable mask and a co-attention distillation to respectively solve the above problems.

## Differentiable Mask

Inspired by CNN compression, where filter-level sparse constraints are imposed along with the training of CNNs (Liu et al. 2017; Huang and Wang 2018; Kang and Han 2020), we devise a mask set  $\mathbf{M} = \{\mathbf{m}_i\}_{i=1}^L$  where  $\mathbf{m}_i = \{m_{i1}, m_{i2}, \dots, m_{in_i}\} \in \mathbb{R}^{n_i}$  is the  $i$ -th layer mask vector. The  $j$ -th element, *i.e.*,  $m_{ij} \in [0, 1]$  will be multiplied with the output of the  $j$ -th filter of  $\mathbf{W}_i^{G_T}$  to scale the convolutional results. Similar to (Liu et al. 2017; Huang and Wang 2018), the network training can be regularized with sparse constraints on the mask  $\mathbf{M}$ . However, their light-weight network architecture has to be manually defined by a pre-given

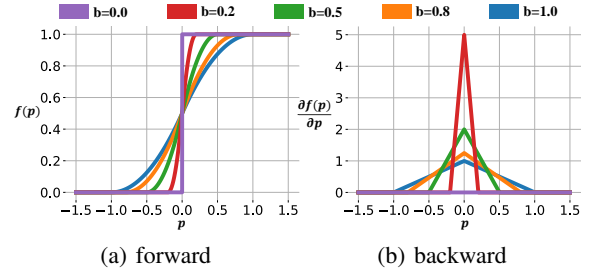


Figure 3: Forward and backward functions of our differentiable mask with varying boundaries.

threshold. In contrast, in this paper, we propose a differentiable mask by regarding each mask  $m_{ij} \in \mathbf{m}_i$  as a differentiable function *w.r.t.* a learnable input  $p_{ij}$ , which in in our implementation is designed as:

$$m_{ij} = f(p_{ij}) = \begin{cases} 0, & \text{if } p_{ij} \leq -b, \\ \frac{1}{2} \cdot \left(\frac{p_{ij}+b}{b}\right)^2, & \text{if } p_{ij} \in (-b, 0], \\ 1 - \frac{1}{2} \cdot \left(\frac{p_{ij}-b}{b}\right)^2, & \text{if } p_{ij} \in (0, b), \\ 1, & \text{if } p_{ij} \geq b, \end{cases} \quad (3)$$

where  $b$  is a boundary, beyond which, the input  $p_{ij}$  will be clipped to 0 or +1. When  $p_{ij} \in (-b, 0]$ , the mask becomes a concave quadratic function; when  $p_{ij} \in (0, b)$ , it becomes a convex quadratic function.

In Fig. 3, we visualize Eq. (3) with varying boundaries. By changing the boundary value, our mask design is shown to be especially advantageous in its high flexibility. Specifically, a large boundary value can be defined at the training beginning training where the quadratic design in Eq. (3) will enable the gradient to be updated in a continuous space ( $m_{ij} \in [0, 1]$ ). Then the gradient will gradually be decreased to zero, where Eq. (3) will be degenerated to a discrete step function ( $m_{ij} \in \{0, 1\}$ ). The light-weight generator can then be derived by removing zero-masked filters at the test stage. Thus, our mask design closes the gap between the discreteness at test time and the continuity during training.

To further relieve the burden on handcrafted boundary adjustment during training, we devise the following training-adaptive strategy

$$b = 1 - \sqrt[3]{e/E}, \quad (4)$$

where  $e$  and  $E$  represent the current training iteration and the total number of training iterations ( $e \in [0, E]$ ), respectively. As can be seen, the boundary will start at 1, which leaves a large boundary margin for gradient updating, and end at 0, which denotes the step function. We adopt the third root sign in Eq. (4) to accelerate the convergence of boundary ( $1 \rightarrow 0$ ), since  $\sqrt[3]{e/E} \geq e/E$  always holds.

**Sparsity Control.** Our designs in Eq. (3) and Eq. (4) can automatically decide which filter to discard (zero-mask) since the introduced parameter  $p_{ij}$  is trainable. To obtain the generator with the desired complexity reduction, a sparse

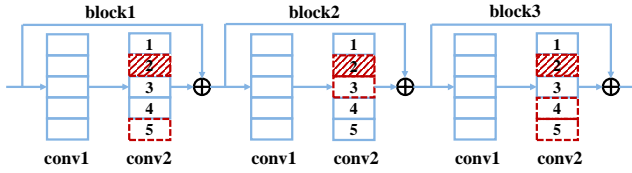


Figure 4: An illustration of adaptive cross-block group sparsity. Filters with the same index in the last convolutional layer of all blocks are divided into a group. As can be seen, when the entire group of masks is 0 (red dotted line), the corresponding filters can be removed (like index 2).

mask is essential. To this end, we formulate our sparse regularization loss for the mask set  $\mathbf{M}$  as follows:

$$\mathcal{L}_{\text{SPA}} = \lambda_{\text{SPA}} \sum_{i=1}^L \sum_{j=1}^{n_i} |p_{ij} + b|, \quad (5)$$

where  $\lambda_{\text{SPA}}$  is the sparse coefficient.

More specifically, our sparse regularization loss aims to force learnable parameter  $p_{ij}$  towards  $-b$ , which will reward a zero mask according to Eq. (3). Different from previous works on CNN compression (Liu et al. 2017; Huang and Wang 2018; Kang and Han 2020), where the exact compression rate can only be obtained after complete training, our training process can be terminated at the point where the sparse rate achieves the desired compression rate, since the zero masks have no gradients and thus will no longer be updated. Thus, the implementation of our sparse design can further reduce the training complexity. Moreover, our sparse constraint is imposed on the learnable parameters rather than the masks directly, which also differentiates our method from existing methods for CNN compression (Liu et al. 2017; Huang and Wang 2018; Kang and Han 2020).

**Pruning Residual Connections.** Residual connections (He et al. 2016) are widely adopted in many current neural networks, including CycleGAN (Zhu et al. 2017), in which the generator network conducts element-wise additions on the feature map outputs of two identity blocks<sup>1</sup>. However, pruning the last convolutional layer in one identity block will result in channel inconsistency among different blocks, which thus paralyzes the entire network.

To solve this, we further propose an adaptive cross-block group sparsity. Specifically, we formulate a set of mask groups  $\mathbf{G} = \{\mathbf{g}_1, \mathbf{g}_2, \dots, \mathbf{g}_{\tilde{n}}\}$ , where  $\tilde{n}$  denotes the filter number in the identity block, and each mask group  $\mathbf{g}_t = \{m_{1t}, m_{2t}, \dots, m_{st}\}$  in which  $s$  is the number of identity blocks in the generator and  $m_{it}$  is the  $t$ -th filter in the last convolutional layer of the  $i$ -th identity block. As shown in Fig. 4, the  $t$ -th mask group consists of the  $t$ -th filters from all identity blocks. It is easy to understand that the channel inconsistency problem can be eliminated by forcing all masks in one group to zeros. To that effect, we devise the following sparse coefficient for the  $t$ -th mask group:

<sup>1</sup>The generator of CycleGAN contains a series of identity blocks and the output channel number of all blocks are the same.

$$\lambda_{\text{GSPA}_t} = \begin{cases} 0, & \text{if } \|\mathbf{g}_t\|_0 = 0, \\ \lambda_{\text{SPA}} \cdot \frac{s}{\|\mathbf{g}_t\|_0}, & \text{otherwise,} \end{cases} \quad (6)$$

where  $\|\cdot\|_0$  denotes the  $\ell_0$ -norm which returns the number of non-zero elements of its input. It is intuitive that a higher sparsity of group  $\mathbf{g}_t$  returns a larger value of  $\lambda_{\text{GSPA}_t}$ . In each training iteration, we calculate  $\lambda_{\text{GSPA}_t}$  first, which is then imposed on its corresponding sparsity term in Eq. (3) to replace the coefficient  $\lambda_{\text{SPA}}$ .

Our motivation of designing Eq. (6) is to assign a stronger sparse constraint on the mask group with a higher sparsity to push all masks to be zero, such that the corresponding filters in all identity blocks can be safely removed without the problem of channel inconsistency.

## Co-Attention Distillation

With the differentiable masks discussed above, we can derive a light-weight generator  $G_S$ , which is then retrained to restore its performance. However, the performance of  $G_S$  is very limited when using traditional adversarial training. According to our experimental observations, the loss of the light-weight generator remains unstable even in the final training iteration, while the discriminator converges to zero quickly. This indicates that  $G_S$  can hardly produce a high-quality image to deceive the discriminator. Thus, auxiliary assistance is necessary to stabilize the adversarial training and boost the performance of  $G_S$ .

Knowledge distillation has emerged as an effective tool in existing GAN compression methods by mimicking intermediate features of a pre-trained teacher GAN in the light-weight generator (Shu et al. 2019; Chen et al. 2020; Fu et al. 2020; Li et al. 2020). However, rather than directly using the intermediate outputs of the teacher model, in this paper, we propose to transfer the attention maps of these intermediate representations, which are demonstrated to contain more valuable information since more details are concentrated there (Zagoruyko and Komodakis 2017).

To this end, for each filter weight  $\mathbf{W}_i^{G_S}$  in the light-weight generator, following (Zagoruyko and Komodakis 2017), we define the attention maps as:

$$\mathbf{A}_i^{G_S} = \sum_{j=1}^{\tilde{c}_i} |\mathbf{O}_i^{G_S}(j, :, :)|^2, \quad (7)$$

where  $\mathbf{O}_i^{G_S}$  is the feature map output of  $\mathbf{W}_i^{G_S}$ . Similarly, we have the attention maps of the teacher generator  $\mathbf{A}_i^{G_T} = \sum_{j=1}^{c_i} |\mathbf{O}_i^{G_T}(j, :, :)|^2$ .

Our goal is to transfer the attention of the pre-trained teacher model to enrich the learning of the light-weight generator. One simple way to achieve this is to minimize the distance between  $\mathbf{A}_i^{G_T}$  and  $\mathbf{A}_i^{G_S}$ . However, this ignores the efficacy of the teacher discriminator  $D_T$ , which has a powerful ability to distinguish images of different domains. Inspired by this, we further consider the attention maps from the teacher discriminator, which are then mixed with all the attention maps of the teacher generator to form the co-attention of the teacher as:

$$\mathbf{A}_i^T = \frac{1}{2}(\mathbf{A}_i^{G_T} + \mathbf{A}_1^{D_T}), \quad (8)$$

where  $\mathbf{A}_1^{D_T} = \sum_{j=1}^{c_1} |\mathbf{O}_1^{D_T}(j, :, :)|^2$  is the attention map of the first convolutional output of the teacher discriminator. To address size inconsistency, we apply Langrange interpolation to the attention map of the discriminator to align it to the attention size of the generator before mixing attentions in Eq. (8). Finally, we derive our objective for co-attention distillation as:

$$\mathcal{L}_{\text{co-ATT}} = \lambda_{\text{co-ATT}} \sum_{i=1}^L \left\| \frac{\mathbf{A}_i^T}{\|\mathbf{A}_i^T\|_2} - \frac{\mathbf{A}_i^{G_S}}{\|\mathbf{A}_i^{G_S}\|_2} \right\|_2^2. \quad (9)$$

where  $\lambda_{\text{co-ATT}}$  is a pre-given hyperparameter. We empirically observe that it is not necessary to distill attention from all layers of the teacher network. Instead, using a small portion can efficiently boost the performance of the light-weight generator, details of which are elaborated in the experiments.

In addition to the proposed co-attention distillation, the high-level information outputs of discriminator are also crucial. Following (Chen et al. 2020), we directly match the last convolutional outputs of the discriminator for the images generated by the pre-trained and light-weight generators as:

$$\mathcal{L}_{\text{FEA}} = \lambda_{\text{FEA}} \frac{1}{n} \sum_{i=1}^n \left\| \tilde{D}_T(G_T(x_i)) - \tilde{D}_T(G_S(x_i)) \right\|_2^2, \quad (10)$$

where  $\lambda_{\text{FEA}}$  is a pre-defined hyperparameter and  $\tilde{D}_T$  returns the feature map outputs from the last convolutional layer of the pre-trained discriminator. Then, our final adversarial training objective can be obtained as:

$$\mathcal{L} = \mathcal{L}_{\text{cGAN}} + \mathcal{L}_{\text{SPA}} + \mathcal{L}_{\text{co-ATT}} + \mathcal{L}_{\text{FEA}}. \quad (11)$$

## Experiments

### Experimental Settings

**Model and Datasets.** To demonstrate the effectiveness of the proposed DMAD, following previous methods (Shu et al. 2019; Chen et al. 2020; Fu et al. 2020; Li et al. 2020), we conduct experiments using CycleGAN (Zhu et al. 2017) and Pix2Pix (Isola et al. 2017). CycleGAN was devised for unpaired image-to-image translation, and is thus evaluated on unpaired datasets, including horse2zebra (Zhu et al. 2017) and summer2winter (Zhu et al. 2017). In contrast, Pix2Pix is a paired image-to-image translation network; thus, we evaluate it on paired datasets, including edges2shoes (Yu and Grauman 2014) and Cityscapes (Cordts et al. 2016). Besides, following the settings in (Li et al. 2020), where the generators are replaced with a separable convolutional network, we also conduct experiments using such a generator structure for fair comparison.

**Evaluation Metrics.** Following previous works for GAN compression (Shu et al. 2019; Fu et al. 2020; Li et al. 2020), we use FID (Frechet Inception Distance) (Heusel et al. 2017) to measure the similarity between real images and generated

images. A lower FID score denotes a higher quality of generated images. On cityscapes, we adopt the DRN-D-105 (Yu, Koltun, and Funkhouser 2017) segmentation model to calculate the mIoU (mean Intersection over Union) for evaluating the quality of generated images. Different from FID, a larger value of mIoU implies a better generated images. Moreover, we also report the MACs, parameters and their corresponding compression rates for an intuitive comparison.

**Implementation Details.** For all experiments, we adopt the Adam optimizer with a tuple of beta values as (0.5, 0.999) for both generator and discriminator. The learning rate is kept to 0.0002 in the beginning and linearly decayed to zero. Following the same settings in (Zhu et al. 2017; Isola et al. 2017), the batch sizes on horse2zebra, summer2winter, edges2shoes and cityscapes are set to 1, 1, 4, and 1, respectively. The hyperparameters  $\lambda_{\text{SPE}}$ ,  $\lambda_{\text{SPA}}$ ,  $\lambda_{\text{co-ATT}}$  and  $\lambda_{\text{FEA}}$  in this paper are set to 10, 0.001, 100, 0.0001 for horse2zebra and summer2winter, and 100, 0.01, 50, 0.0001 for edges2shoes and cityscapes, respectively.

In terms of co-attention distillation, we split the CycleGAN generator into five equal groups (each residual block is regarded as one layer), and then select per-group feature map outputs to extract attention maps. As for the Pix2Pix generator, we extract attention maps from the second, fourth, twelfth, and fourteenth convolutional layers.

## Experimental Results

**Quantitative Results.** As can be seen from Tab. 1, for CycleGAN compression, our DMAD can achieve a comparable (on zebra2horse, summer2winter and winter2summer) or even a much smaller (on horse2zebra) FID metric in comparison to the original model, while still also obtaining a significant reduction in model complexity of 13.2 – 23.6 $\times$  in MACs and 25.1 – 47.1 $\times$  in parameters. Similarly, for Pix2Pix compression, the proposed DMAD results in 4.24 – 6.22 $\times$  MACs compression and 25.5 – 100.7 $\times$  reductions of parameters, while obtaining a smaller FID value on edges2shoes and similar mIoU performance on cityscapes when compared to the full model. Besides, in contrast to the recent state-of-the-arts (Shu et al. 2019; Fu et al. 2020; Li et al. 2020), our compressed models have fewer MACs and parameters, while still retaining a better metric performance in most cases. This demonstrates the effectiveness of our DMAD in reducing GAN complexity.

**Adaptive Cross-Block Group Sparsity.** Tab. 2 displays the effectiveness of our adaptive cross-block group sparsity for residual connections in CycleGAN. We remove the co-attention distillation to exclude its effect. We can see that our adaptive cross-block group sparsity can effectively reduce the model redundancy with better image generation. Thus, this clearly demonstrates the necessity of pruning residual connections and efficacy of our adaptive sparsity strategy.

**Component Analysis.** In Tab. 3, we show the impact of different components in our DMAD including inheriting weights from the searched model, generator attention, our proposed co-attention, and high-level information of discriminator. As can be seen from the table, inheriting weights

Model	Task	Method	MACs (CR)	Parameters (CR)	FID( $\downarrow$ )	mIoU( $\uparrow$ )
CycleGAN	horse2zebra	Original	56.8G (1.0 $\times$ )	11.3M (1.0 $\times$ )	74.04	-
		Co-Evolution (Shu et al. 2019)	13.4G (4.2 $\times$ )	-	96.15	-
		AutoGAN (Fu et al. 2020)	6.39G (8.9 $\times$ )	-	83.60	-
	zebra2horse	<b>DMAD (Ours)</b>	<b>3.97G (14.3<math>\times</math>)</b>	<b>0.42M (26.9<math>\times</math>)</b>	<b>62.41</b>	-
		GAN-Compression* (Li et al. 2020)	2.67G (21.3 $\times$ )	0.34M (33.2 $\times$ )	64.95	-
		<b>DMAD* (Ours)</b>	<b>2.41G (23.6<math>\times</math>)</b>	<b>0.28M (40.4<math>\times</math>)</b>	<b>62.96</b>	-
CycleGAN	summer2winter	Original	56.8G (1.0 $\times$ )	11.3M (1.0 $\times$ )	137.8	-
		Co-Evolution (Shu et al. 2019)	13.1G (4.3 $\times$ )	-	157.9	-
		AutoGAN (Fu et al. 2020)	4.84G (11.7 $\times$ )	-	137.2	-
	winter2summer	<b>DMAD (Ours)</b>	<b>3.50G (16.2<math>\times</math>)</b>	<b>0.30M (37.7<math>\times</math>)</b>	<b>139.3</b>	-
		Original	56.8G (1.0 $\times$ )	11.3M (1.0 $\times$ )	79.12	-
		Co-Evolution (Shu et al. 2019)	11.1G (5.1 $\times$ )	-	78.58	-
Pix2Pix	edges2shoes	AutoGAN (Fu et al. 2020)	4.34G (13.1 $\times$ )	-	78.33	-
		<b>DMAD (Ours)</b>	<b>3.18G (17.9<math>\times</math>)</b>	<b>0.24M (47.1<math>\times</math>)</b>	<b>78.24</b>	-
		Original	56.8G (1.0 $\times$ )	11.3M (1.0 $\times$ )	73.31	-
	cityscapes	Pix2Pix 0.5 $\times$	4.65G (4.0 $\times$ )	13.6M (4.0 $\times$ )	52.02	-
		<b>DMAD (Ours)</b>	<b>2.99G (6.22<math>\times</math>)</b>	<b>2.13M (25.5<math>\times</math>)</b>	<b>46.95</b>	-
		GAN-Compression* (Li et al. 2020)	4.81G (3.8 $\times$ )	0.7M (77.7 $\times$ )	26.60	-
	cityscapes	<b>DMAD* (Ours)</b>	<b>4.30G (4.32<math>\times</math>)</b>	<b>0.54M (100.7<math>\times</math>)</b>	<b>24.08</b>	-
		Original	18.6G (1.0 $\times$ )	54.4M (1.0 $\times$ )	34.31	-
		Pix2Pix $\times 0.5$	4.65G (4.0 $\times$ )	13.6M (4.0 $\times$ )	-	42.71
		<b>DMAD (Ours)</b>	<b>3.96G (4.70<math>\times</math>)</b>	<b>1.73M (31.4<math>\times</math>)</b>	-	<b>39.02</b>
		GAN-Compression* (Li et al. 2020)	5.66G (3.28 $\times$ )	0.71M (76.6 $\times$ )	-	40.53
		<b>DMAD* (Ours)</b>	<b>4.39G (4.24<math>\times</math>)</b>	<b>0.55M (98.9<math>\times</math>)</b>	-	<b>41.47</b>

Table 1: Quantitative comparison with other GAN compression methods. \* indicates that a generator with separable convolutions is adopted, following (Li et al. 2020). CR stands for the compression rate.

Task	Adaptive	PR	MACs	FID( $\downarrow$ )
horse2zebra	$\times$	0.33	6.80G	70.77
	$\checkmark$	0.72	3.97G	66.23
zebra2horse	$\times$	0.39	5.43G	147.7
	$\checkmark$	0.69	3.50G	140.2

Table 2: Performance comparison with/without our adaptive cross-block group sparsity on horse2zebra and zebra2horse. PR represents the pruning rate of residual blocks.

(Finetune) from the pre-trained model does benefit to the quality of generated images. Then, by considering the generator attention (G-Attention), the FID metric is further reduced which implicates the effectiveness of distilling attention mechanism in improving the performance of light-weight generator. Besides, with attention maps from the discriminator (co-Attention), the generated images are further improved with FID decreasing from 66.26 to 64.97. Such a performance gain verifies the efficacy of our proposed co-attention distillation. Moreover, the distilling high-level information of discriminator (D-Distill) also benefits the generated images where the FID decreases from 67.26 to 65.38. By utilizing all of these components, our DMAD obtains the best FID value of 62.41.

Model	Inherit Weights	$\mathcal{L}_{\text{co-ATT}}$	$\mathcal{L}_{\text{FEA}}$	FID( $\downarrow$ )
Scratch				69.50
Finetune	$\checkmark$			67.26
G-Attention	$\checkmark$			66.26
co-Attention	$\checkmark$	$\checkmark$		64.97
D-Distill	$\checkmark$		$\checkmark$	65.38
DMAD(ours)	$\checkmark$	$\checkmark$	$\checkmark$	62.41

Table 3: The impact of different components on horse2zebra tasks. G-Attention denotes that only generator attentions are applied. D-Distill denotes distillation of high-level information from discriminator.

**Visualization.** Fig.5 shows the visualization results on horse2zebra, zebra2horse, and cityscapes. As can be seen, our method obtains similar or even better visual results, with higher MACs reductions. Compared with AutoGAN (Fu et al. 2020), where the zebra stripes very sharp, and Co-evolution (Shu et al. 2019), where clear softening marks are generated around the horse, our generated images are more vivid and authentic. On cityscapes, we compress the Pix2Pix generator by 4.7 $\times$ , while still achieving a similar output as the original generator.

**Compression and Acceleration.** The pruning rates of each layer searched by the differential mask in Pix2Pix on



Figure 5: Visualization of our DMAD. The first two lines are the results on horse2zebra and zebra2horse, comparing with Co-Evolution (Shu et al. 2019) and AutoGAN (Fu et al. 2020). The third line displays the results on cityscapes.

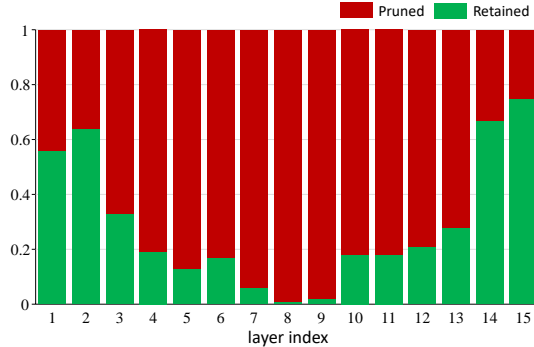


Figure 6: Per-layer pruning rate of Pix2Pix generator on cityscapes.

the cityscapes dataset as shown in Fig.6. Pix2Pix uses U-Net as generator, we find that, as the number of U-Net network layers increases, the overall pruning rate looks like an letter U. The first few layers extract valid input information, while the last few layers construct the final generated images, so these layers are vital for generating high-quality images. Compared to these layers, the other layers of U-Net are less important. This is especially true for the most intermediate network layer, whose output feature map size is only  $1 \times 1$ , and has little impact on the final  $256 \times 256$  image. Thus, these layers can reach a higher pruning rate. The results reflect that the differential mask can adaptively prune

according to the contribution of each layer.

During model deployment, the actual acceleration effect on the hardware is more critical than the reduction of theoretical calculations. We compare the actual acceleration effect between the original model and the compressed model on different types processors (*i. e.* CPUs and GPUs). On the horse2zebra task, it takes 440ms for the original model to process one image using an Intel Xeon CPU E5-2690 CPU and 7.1ms on one GTX1080TI GPU. The compressed model requires 76.3ms and 5.8ms to process an image on a CPU and a GPU, respectively. It achieves  $5.8 \times$  and  $1.2 \times$  acceleration on a CPU and a GPU, respectively. Due to the powerful parallel processing capabilities of GPUs, the acceleration effect on the GPU is not as obvious as on the CPU. The gap between the realistic and theoretical speed-up ratio may come from the limitations of IO decay, data transmission, *etc.*

## Conclusion

In this work, we introduce a novel framework for GAN compression, termed DMAD. First, we propose a differentiable mask to carry out architecture search for a light-weight generator in a training-adaptive manner. An adaptive cross-block group sparsity is then further incorporated for block-level pruning. Second, we distill attention maps extracted from both the generator and discriminator of the pre-trained model to the light-weight generator, which makes training more stable and yields superior performance. Extensive experiments demonstrate the ability of our proposed DMAD method in preserving visual quality of generated images.

## References

Chen, H.; Wang, Y.; Shu, H.; Wen, C.; Xu, C.; Shi, B.; Xu, C.; and Xu, C. 2020. Distilling portable Generative Adversarial Networks for Image Translation. In *Proceedings of the AAAI Conference on Artificial Intelligence (AAAI)*, 3585–3592.

Cordts, M.; Omran, M.; Ramos, S.; Rehfeld, T.; Enzweiler, M.; Benenson, R.; Franke, U.; Roth, S.; and Schiele, B. 2016. The cityscapes dataset for semantic urban scene understanding. In *Proceedings of the IEEE conference on Computer Vision and Pattern Recognition (CVPR)*, 3213–3223.

Denil, M.; Shakibi, B.; Dinh, L.; Ranzato, M.; and De Freitas, N. 2013. Predicting parameters in deep learning. In *Proceedings of the Advances in Neural Information Processing Systems (NeurIPS)*, 2148–2156.

Ding, X.; Zhou, X.; Guo, Y.; Han, J.; Liu, J.; et al. 2019. Global sparse momentum sgd for pruning very deep neural networks. In *Proceedings of the Advances in Neural Information Processing Systems (NeurIPS)*, 6382–6394.

Frankle, J.; and Carbin, M. 2019. The lottery ticket hypothesis: Finding sparse, trainable neural networks. In *Proceedings of the International Conference of Learning Representation (ICLR)*.

Fu, Y.; Chen, W.; Wang, H.; Li, H.; Lin, Y.; and Wang, Z. 2020. AutoGAN-Distiller: Searching to Compress Generative Adversarial Networks. In *Proceedings of the International Conference on Machine Learning (ICML)*.

Goodfellow, I.; Pouget-Abadie, J.; Mirza, M.; Xu, B.; Warde-Farley, D.; Ozair, S.; Courville, A.; and Bengio, Y. 2014. Generative adversarial nets. In *Proceedings of the Advances in Neural Information Processing Systems (NeurIPS)*, 2672–2680.

Han, S.; Pool, J.; Tran, J.; and Dally, W. 2015. Learning both weights and connections for efficient neural network. In *Proceedings of the Advances in Neural Information Processing Systems (NeurIPS)*, 1135–1143.

Hayashi, K.; Yamaguchi, T.; Sugawara, Y.; and Maeda, S.-i. 2019. Exploring Unexplored Tensor Network Decompositions for Convolutional Neural Networks. In *Proceedings of the Advances in Neural Information Processing Systems (NeurIPS)*, 5552–5562.

He, K.; Zhang, X.; Ren, S.; and Sun, J. 2016. Deep residual learning for image recognition. In *Proceedings of the IEEE conference on Computer Vision and Pattern Recognition (CVPR)*, 770–778.

Heusel, M.; Ramsauer, H.; Unterthiner, T.; Nessler, B.; and Hochreiter, S. 2017. Gans trained by a two time-scale update rule converge to a local nash equilibrium. In *Proceedings of the Advances in Neural Information Processing Systems (NeurIPS)*, 6626–6637.

Hinton, G.; Vinyals, O.; and Dean, J. 2015. Distilling the knowledge in a neural network. *arXiv preprint arXiv:1503.02531* .

Huang, Z.; and Wang, N. 2018. Data-driven sparse structure selection for deep neural networks. In *Proceedings of the European Conference on Computer Vision (ECCV)*, 304–320.

Iandola, F. N.; Han, S.; Moskewicz, M. W.; Ashraf, K.; Dally, W. J.; and Keutzer, K. 2016. SqueezeNet: AlexNet-level accuracy with 50x fewer parameters and; 0.5 MB model size. *arXiv preprint arXiv:1602.07360* .

Isola, P.; Zhu, J.-Y.; Zhou, T.; and Efros, A. A. 2017. Image-to-image translation with conditional adversarial networks. In *Proceedings of the IEEE conference on Computer Vision and Pattern Recognition (CVPR)*, 1125–1134.

Kang, M.; and Han, B. 2020. Operation-Aware Soft Channel Pruning using Differentiable Masks. In *Proceedings of the International Conference on Machine Learning (ICML)*.

LeCun, Y.; Denker, J. S.; and Solla, S. A. 1990. Optimal brain damage. In *Proceedings of the Advances in Neural Information Processing Systems (NeurIPS)*, 598–605.

Leng, C.; Li, H.; Zhu, S.; and Jin, R. 2018. Extremely low bit neural network: Squeeze the last bit out with admm. In *Proceedings of the AAAI Conference on Artificial Intelligence (AAAI)*, 3466–3473.

Li, M.; Lin, J.; Ding, Y.; Liu, Z.; Zhu, J.-Y.; and Han, S. 2020. Gan compression: Efficient architectures for interactive conditional gans. In *Proceedings of the IEEE conference on Computer Vision and Pattern Recognition (CVPR)*, 5284–5294.

Lin, M.; Ji, R.; Wang, Y.; Zhang, Y.; Zhang, B.; Tian, Y.; and Shao, L. 2020a. HRank: Filter Pruning using High-Rank Feature Map. In *Proceedings of the IEEE conference on Computer Vision and Pattern Recognition (CVPR)*, 1529–1538.

Lin, M.; Ji, R.; Xu, Z.; Zhang, B.; Wang, Y.; Wu, Y.; Huang, F.; and Lin, C.-W. 2020b. Rotated Binary Neural Network. In *Proceedings of the Advances in Neural Information Processing Systems (NeurIPS)*.

Lin, M.; Ji, R.; Zhang, Y.; Zhang, B.; Wu, Y.; and Tian, Y. 2020c. Channel Pruning via Automatic Structure Search. In *Proceedings of the International Joint Conference on Artificial Intelligence (IJCAI)*, 673–679.

Liu, Z.; Li, J.; Shen, Z.; Huang, G.; Yan, S.; and Zhang, C. 2017. Learning efficient convolutional networks through network slimming. In *Proceedings of the IEEE International Conference on Computer Vision (ICCV)*, 2736–2744.

Radford, A.; Metz, L.; and Chintala, S. 2015. Unsupervised representation learning with deep convolutional generative adversarial networks. *arXiv preprint arXiv:1511.06434* .

Romero, A.; Ballas, N.; Kahou, S. E.; Chassang, A.; Gatta, C.; and Bengio, Y. 2015. Fitnets: Hints for thin deep nets. In *Proceedings of the International Conference of Learning Representation (ICLR)*.

Sandler, M.; Howard, A.; Zhu, M.; Zhmoginov, A.; and Chen, L.-C. 2018. Mobilenetv2: Inverted residuals and linear bottlenecks. In *Proceedings of the IEEE conference on*

*Computer Vision and Pattern Recognition (CVPR)*, 4510–4520.

Shu, H.; Wang, Y.; Jia, X.; Han, K.; Chen, H.; Xu, C.; Tian, Q.; and Xu, C. 2019. Co-evolutionary compression for unpaired image translation. In *Proceedings of the IEEE International Conference on Computer Vision (ICCV)*, 3235–3244.

Wang, Y.; Zhang, X.; Xie, L.; Zhou, J.; Su, H.; Zhang, B.; and Hu, X. 2020. Pruning from Scratch. In *Proceedings of the AAAI Conference on Artificial Intelligence (AAAI)*, 12273–12280.

Yim, J.; Joo, D.; Bae, J.; and Kim, J. 2017. A gift from knowledge distillation: Fast optimization, network minimization and transfer learning. In *Proceedings of the IEEE conference on Computer Vision and Pattern Recognition (CVPR)*, 4133–4141.

Yu, A.; and Grauman, K. 2014. Fine-grained visual comparisons with local learning. In *Proceedings of the IEEE conference on Computer Vision and Pattern Recognition (CVPR)*, 192–199.

Yu, F.; Koltun, V.; and Funkhouser, T. 2017. Dilated residual networks. In *Proceedings of the IEEE conference on Computer Vision and Pattern Recognition (CVPR)*, 472–480.

Zagoruyko, S.; and Komodakis, N. 2017. Paying more attention to attention: Improving the performance of convolutional neural networks via attention transfer. In *Proceedings of the International Conference of Learning Representation (ICLR)*.

Zhang, X.; Zhou, X.; Lin, M.; and Sun, J. 2018. Shufflenet: An extremely efficient convolutional neural network for mobile devices. In *Proceedings of the IEEE conference on Computer Vision and Pattern Recognition (CVPR)*, 6848–6856.

Zhu, J.-Y.; Park, T.; Isola, P.; and Efros, A. A. 2017. Unpaired image-to-image translation using cycle-consistent adversarial networks. In *Proceedings of the IEEE International Conference on Computer Vision (ICCV)*, 2223–2232.

Zhuang, Z.; Tan, M.; Zhuang, B.; Liu, J.; Guo, Y.; Wu, Q.; Huang, J.; and Zhu, J. 2018. Discrimination-aware channel pruning for deep neural networks. In *Proceedings of the Advances in Neural Information Processing Systems (NeurIPS)*, 875–886.